Supplement of Earth Surf. Dynam., 13, 437–454, 2025
https://doi.org/10.5194/esurf-13-437-2025-supplement

Supplement of

Investigating the celerity of propagation for small perturbations and dispersive sediment aggradation under a supercritical flow

Hasan Eslami et al.

Correspondence to: Alessio Radice (alessio.radice@polimi.it)

S1. Governing equations and eigenvalue analysis for non-negligible c_s (Morris and Williams' approach)

Morris and Williams (1996) argued that an assumption of negligible solid concentration is not appropriate for many natural streams and, therefore, determined the eigenvalues of a system of equations considering a finite c_s. The continuity and momentum equations of the mixture and the continuity equation for the sediment in Morris and Williams' approach are as follows:

$$\begin{cases} \frac{\partial(uh)}{\partial x}+\frac{\partial h}{\partial t}+\frac{\partial z_b}{\partial t}=0 \\ \frac{\partial u}{\partial t}+u\frac{\partial u}{\partial x}+g\frac{\partial h}{\partial x}+\frac{(\rho_s-\rho)gh}{2\rho_m}\frac{\partial c_s}{\partial x}-\frac{[(1-p_0)\rho_s+p_0\rho]u}{\rho_m h}\frac{\partial z_b}{\partial t}+g\frac{\partial z_b}{\partial x}=-gS_f \\ \frac{\partial(uhc_s)}{\partial x}+\frac{\partial(hc_s)}{\partial t}+(1-p_0)\frac{\partial z_b}{\partial t}=0 \end{cases} \tag{S1}$$

where, $c_s=q_s/(q_s+q)$, $\rho_m=c_s\rho_s+(1-c_s)\rho$ is the density of the mixture, and the other symbols are as defined in the manuscript. Since the solid concentration is not negligible, the water and sediment discharge per unit width are obtained from the following equations (assuming that the solid particles move at the same velocity as water):

$$q=uh(1-c_s) \tag{S2}$$

$$q_s=uhc_s \tag{S3}$$

In system (S1), one can substitute the terms $\partial c_s/\partial x$ and $\partial c_s/\partial t$ with following equations:

$$\frac{\partial c_s}{\partial x}=\frac{\partial c_s}{\partial u}\frac{\partial u}{\partial x}+\frac{\partial c_s}{\partial h}\frac{\partial h}{\partial x} \tag{S4}$$

$$\frac{\partial c_s}{\partial t}=\frac{\partial c_s}{\partial u}\frac{\partial u}{\partial t}+\frac{\partial c_s}{\partial h}\frac{\partial h}{\partial t} \tag{S5}$$

and thus modify (S1) as below:

$$\begin{cases} u\frac{\partial h}{\partial x}+h\frac{\partial u}{\partial x}+\frac{\partial h}{\partial t}+\frac{\partial z_b}{\partial t}=0 \\ \frac{1}{g}\frac{\partial u}{\partial t}+\frac{u}{g}\frac{\partial u}{\partial x}+\frac{\partial h}{\partial x}+Ah\left(\frac{\partial c_s}{\partial u}\frac{\partial u}{\partial x}+\frac{\partial c_s}{\partial h}\frac{\partial h}{\partial x}\right)-B\frac{u}{gh}\frac{\partial z_b}{\partial t}+\frac{\partial z_b}{\partial x}=-S_f \\ uc_s\frac{\partial h}{\partial x}+hc_s\frac{\partial u}{\partial x}+uh\left(\frac{\partial c_s}{\partial u}\frac{\partial u}{\partial x}+\frac{\partial c_s}{\partial h}\frac{\partial h}{\partial x}\right)+c_s\frac{\partial h}{\partial t}+h\left(\frac{\partial c_s}{\partial u}\frac{\partial u}{\partial t}+\frac{\partial c_s}{\partial h}\frac{\partial h}{\partial t}\right)+ \\ (1-p_0)\frac{\partial z_b}{\partial t}=0 \end{cases} \tag{S6}$$

where, $A=(\rho_s-\rho)/(2\rho_m)$, and $B=\big((1-p_0)\rho_s+p_0\rho\big)/\rho_m$, are dimensionless parameters. In order to find the eigenvalues of this system, it is also needed to compute the differential of u, h, and z_b:

$$\frac{\partial u}{\partial t}dt+\frac{\partial u}{\partial x}dx=du \tag{S7}$$

$$\frac{\partial h}{\partial t}dt+\frac{\partial h}{\partial x}dx=dh \tag{S8}$$

$$\frac{\partial z_b}{\partial t}dt+\frac{\partial z_b}{\partial x}dx=dz_b \tag{S9}$$

Now, the eigenvalues of the system can be obtained by equalizing the determinant of the set of system (S6) to zero, accounting for equations (S7)-(S9) (De Vries 1965; Cunge et al. 1980):

$$
\begin{vmatrix}
h\frac{\partial c_s}{\partial u} & h\left(c_s + u\frac{\partial c_s}{\partial u}\right) & c_s + h\frac{\partial c_s}{\partial h} & u\left(c_s + h\frac{\partial c_s}{\partial h}\right) & (1-p_0) & 0 \\
0 & h & 1 & u & 1 & 0 \\
\frac{1}{g} & \frac{u}{g} + Ah\frac{\partial c_s}{\partial u} & 0 & 1 + Ah\frac{\partial c_s}{\partial h} & -\frac{Bh}{gh} & 1 \\
dt & dx & 0 & 0 & 0 & 0 \\
0 & 0 & dt & dx & 0 & 0 \\
0 & 0 & 0 & 0 & dt & dx
\end{vmatrix} = 0 \tag{S10}
$$

The characteristic polynomial equation was obtained by Morris and Williams (1996) as follows:

$$
\lambda^3 \left\{Bu\frac{\partial c_s}{\partial u} - h\frac{\partial c_s}{\partial h} - [c_s - (1-p_0)]\right\} + \lambda^2 \left(\{Agh[c_s - (1-p_0)] - 2Bu^2\}\frac{\partial c_s}{\partial u} + (2+B)uh\frac{\partial c_s}{\partial h} + 2u[c_s - (1-p_0)]\right) + \lambda\left[(Bu^3 - ugh\{1 + A[c_s - (1-p_0)]\})\frac{\partial c_s}{\partial u} - \left((1+B)u^2h - gh^2\{1 + A[c_s - (1-p_0)]\}\right)\frac{\partial c_s}{\partial h} - (u^2 - gh)[c_s - (1-p_0)]\right] + ugh\left(u\frac{\partial c_s}{\partial u} - h\frac{\partial c_s}{\partial h}\right) = 0 \tag{S11}
$$

and in dimensionless form as below:

$$
\acute{\lambda}^3 \left\{Bu\frac{\partial c_s}{\partial u} - h\frac{\partial c_s}{\partial h} - [c_s - (1-p_0)]\right\} + \acute{\lambda}^2 \left(\{AFr^{-2}[c_s - (1-p_0)] - 2B\}u\frac{\partial c_s}{\partial u} + (2+B)h\frac{\partial c_s}{\partial h} + 2[c_s - (1-p_0)]\right) + \acute{\lambda}\left[(B - Fr^{-2}\{1 + A[c_s - (1-p_0)]\})u\frac{\partial c_s}{\partial u} - (1 + B - Fr^{-2}\{1 + A[c_s - (1-p_0)]\})h\frac{\partial c_s}{\partial h} + (Fr^{-2} - 1)[c_s - (1-p_0)]\right] + Fr^{-2}\left(u\frac{\partial c_s}{\partial u} - h\frac{\partial c_s}{\partial h}\right) = 0 \tag{S12}
$$

where, $\acute{\lambda} = \lambda/u$ = relative celerity. By solving this cubic equation, one can determine the three celerities of the system exactly.

S2. Results for the performed aggradation experiments

During the experimental campaign including the experiment presented in the manuscript, twenty-five aggradation experiments were conducted, with the key parameters summarized in Table S1. The symbols used include: T, representing the experiment duration; S_0, the initial slope of the channel; Q, the water discharge; Q_{s-in}, the sediment inflow discharge; Q_{s0}, the sediment transport capacity of the initial flow; and Lr, a load ratio defined as Q_{s-in}/Q_{s0}, where $Lr > 1$ ensures the occurrence of aggradation during each run. H and U denote water depth and velocity, respectively, calculated using the Gauckler-Strickler formula under the assumption of uniform flow. $Fr = U/\sqrt{gH}$ represents the Froude number, and $Re = \rho UH/\mu$ is the Reynolds number, where ρ and μ are density and dynamic viscosity of water. $\overline{C_s}$ represents the average value of sediment concentration during each run. Lastly, P is the Pearson's correlation coefficient between the Froude number and the dimensionless local and instantaneous celerity of propagation of aggradation wave, C/u, for each run. The experiments are classified into two categories based on the initial channel slope (1.37% and 2.20%), seven categories based on water discharge (ranging from 0.003 m^3/s to 0.009 m^3/s), and five categories based on the load ratio, with representative values of 1.55, 1.85, 2.15, 2.7, and 3.2. The experiment featured in the paper is AE16, and for the sake of completeness, its results will also be presented in this supplemental file.

As shown in Table S1, the value of $\overline{C_s}$ in all experiments exceeded 0.01, indicating that the solid concentration was not negligible according to the criteria proposed by De Vries (1965), with a maximum C_s of 0.002, and Garegnani et al. (2011, 2013), with a maximum C_s of 0.01. Furthermore, $\overline{C_s}$ remained below the maximum threshold of 0.05 suggested by Armanini et al. (2009) for the validity of the quasi-two-phase approach.

Table S1. Parameters of the aggradation experiments performed in the experimental campaign.

Run	T (s)	S_0 (%)	Q (m^3/s)	Q_{s-in} (m^3/s)	Q_{s0} (m^3/s)	Lr	H (m)	U (m/s)	Fr	Re	$\overline{c_s}$	P
AE1	1019	1.37	0.003	1.14E-04	6.25E-05	1.83	0.019	0.518	1.190	8860	0.029	-0.33
AE2	812	1.37	0.003	1.28E-04	6.25E-05	2.05	0.019	0.518	1.190	8860	0.021	-0.26
AE3	774	1.37	0.004	1.25E-04	8.05E-05	1.56	0.023	0.576	1.209	11551	0.019	-0.31
AE4	686	1.37	0.004	1.68E-04	8.05E-05	2.09	0.023	0.576	1.209	11551	0.019	-0.40
AE5	559	1.37	0.004	2.27E-04	8.05E-05	2.81	0.023	0.576	1.209	11551	0.030	-0.39
AE6	638	1.37	0.005	1.55E-04	9.59E-05	1.61	0.027	0.625	1.221	14150	0.021	-0.25
AE7	452	1.37	0.005	1.99E-04	9.59E-05	2.07	0.027	0.625	1.221	14150	0.028	-0.03
AE8	482	1.37	0.005	2.48E-04	9.59E-05	2.58	0.027	0.625	1.221	14150	0.027	-0.18
AE9	442	1.37	0.005	3.03E-04	9.59E-05	3.16	0.027	0.625	1.221	14150	0.019	-0.31
AE10	594	1.37	0.006	1.70E-04	1.20E-04	1.42	0.030	0.667	1.230	16668	0.019	-0.09
AE11	462	1.37	0.006	2.62E-04	1.20E-04	2.19	0.030	0.667	1.230	16668	0.025	-0.14
AE12	384	1.37	0.006	3.30E-04	1.20E-04	2.76	0.030	0.667	1.230	16668	0.027	-0.27
AE13	363	1.37	0.006	3.94E-04	1.20E-04	3.29	0.030	0.667	1.230	16668	0.028	-0.22
AE14	567	1.37	0.007	1.90E-04	1.33E-04	1.43	0.033	0.705	1.236	19113	0.015	-0.28
AE15	368	1.37	0.007	2.77E-04	1.33E-04	2.09	0.033	0.705	1.236	19113	0.024	-0.30
AE16	316	1.37	0.007	4.28E-04	1.33E-04	3.22	0.033	0.705	1.236	19113	0.032	-0.40
AE17	388	1.37	0.008	2.57E-04	1.60E-04	1.61	0.036	0.738	1.240	21492	0.025	-0.47
AE18	371	1.37	0.008	2.64E-04	1.60E-04	1.65	0.036	0.738	1.240	21492	0.024	-0.26
AE19	344	1.37	0.008	3.46E-04	1.60E-04	2.16	0.036	0.738	1.240	21492	0.030	-0.45
AE20	276	1.37	0.008	4.42E-04	1.60E-04	2.76	0.036	0.738	1.240	21492	0.035	-0.26
AE21	319	1.37	0.009	2.92E-04	1.87E-04	1.56	0.039	0.769	1.244	23810	0.025	-0.32
AE22	275	1.37	0.009	4.16E-04	1.87E-04	2.23	0.039	0.769	1.244	23810	0.030	-0.36
AE23	496	2.20	0.004	2.52E-04	1.43E-04	1.76	0.020	0.669	1.513	11769	0.039	-0.13
AE24	422	2.20	0.005	2.80E-04	1.83E-04	1.53	0.023	0.726	1.531	14455	0.036	-0.34
AE25	375	2.20	0.006	3.27E-04	2.13E-04	1.53	0.026	0.776	1.544	17068	0.032	-0.21

The scatter plots showing the relationships between Fr and C/u, Fr and λ_i/u, and λ_i/u and C/u are presented for experiments AE12, AE16, AE17, AE19, and AE24. These experiments were selected because they encompass various loading ratios and initial slopes. Specifically, AE12, AE16, AE17 and AE19 represent experiments with load ratios of approximately 2.7, 3.2, 1.55 and 2.15, respectively, and with an initial slope of 1.37%; AE24 represents the experiments with an initial slope of 2.20% and a load ratio of approximately 1.55.

In the following pages, for each of the aforementioned experiments a table is first provided presenting the Pearson's correlation coefficient values to quantify the strength of the correlation between C/u and Fr and between C/u and λ_i/u. The table is followed by scatter plots illustrating the relationship between Fr and C/u, Fr and λ_i/u, and λ_i/u and C/u during the runs, as documented in the manuscript for AE16. It is worth mentioning that since celerity approaches zero once equilibrium is reached, only the data points up to the equilibrium time are included in the plots. The equilibrium times for the experiments AE12, AE16, AE17, AE19, and AE24 are 360 s, 190 s, 290 s, 340 s, and 300 s, respectively.

Table S2. Pearson's correlation coefficient between the dimensionless local and instantaneous celerity of the aggradation wave and the Froude number, as well as the dimensionless eigenvalues, for experiment AE12.

AE12		Goutière et al. (2008)			Morris and Williams (1996)		
	Fr	λ_1/u	λ_2/u	λ_3/u	λ_1/u	λ_2/u	λ_3/u
C/u	-0.27	0.33	-0.41	-0.30	0.33	-0.38	-0.30

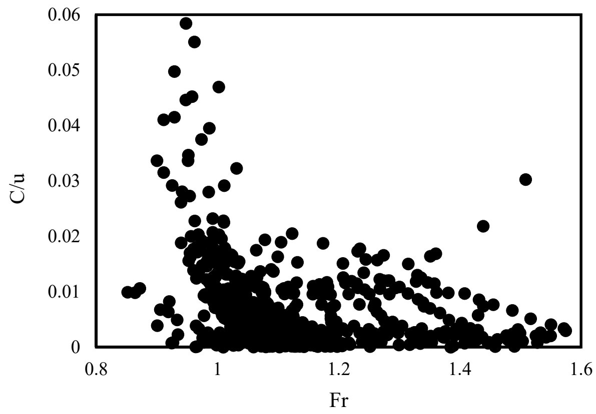

Figure S1. Scatter plot showing the correlation between the Froude number and the dimensionless local and instantaneous celerity of aggradation wave for experiment AE12.

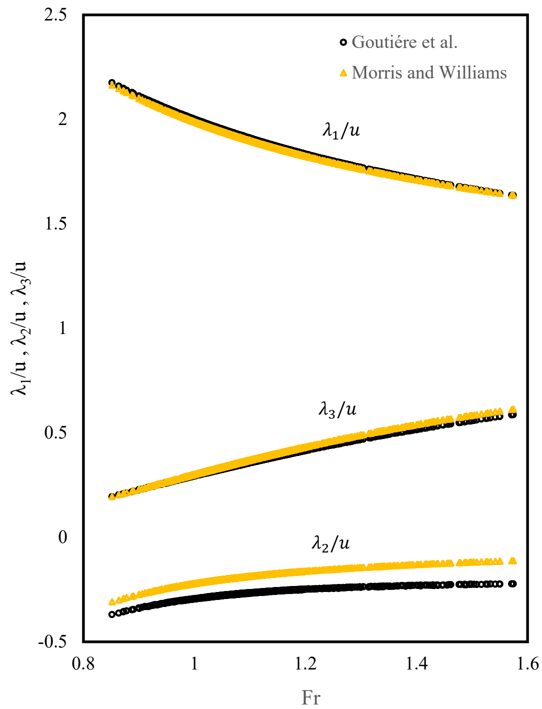

Figure S2. Scatter plot showing the correlation between the Froude number and the dimensionless eigenvalues for experiment AE12.

(a)

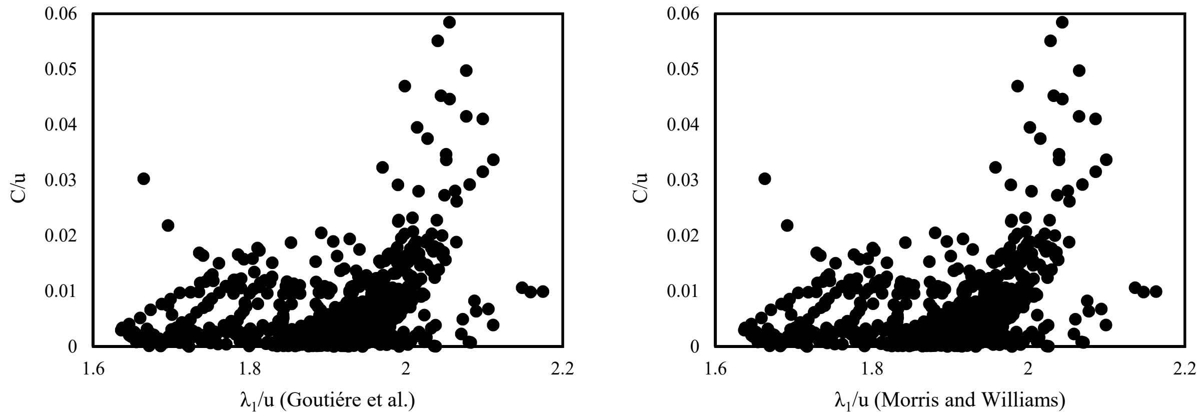

(b)

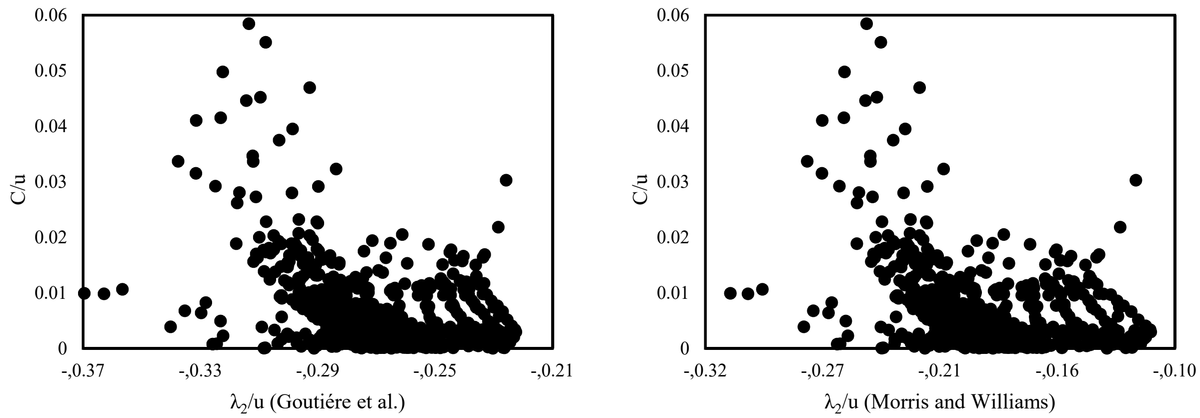

(c)

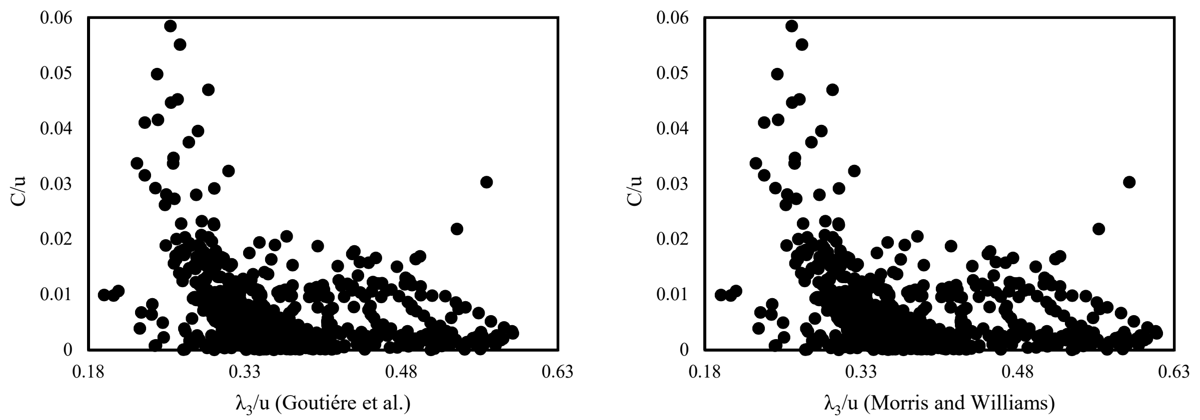

Figure S3. Scatter plots showing the correlations between the dimensionless eigenvalues and the dimensionless celerity of the aggradation wave for experiment AE12. The left graphs are obtained from the approximated solutions proposed by Goutière et al. (2008) and, the right graphs are derived from the exact solution of Morris and Williams' (1996) approach.

Table S3. Pearson's correlation coefficient between the dimensionless local and instantaneous celerity of the aggradation wave and the Froude number, as well as the dimensionless eigenvalues, for experiment AE16.

AE16		Goutière et al. (2008)			Morris and Williams (1996)		
	Fr	λ_1/u	λ_2/u	λ_3/u	λ_1/u	λ_2/u	λ_3/u
C/u	-0.40	0.46	-0.62	-0.42	0.46	-0.52	-0.43

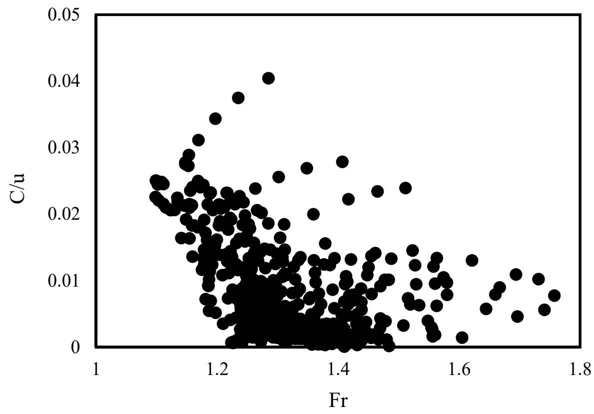

Figure S4. Scatter plot showing the correlation between the Froude number and the dimensionless local and instantaneous celerity of aggradation wave for experiment AE16.

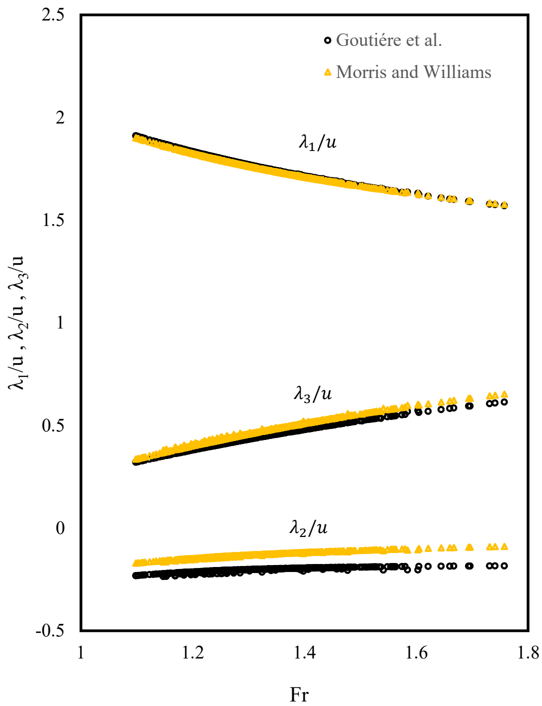

Figure S5. Scatter plot showing the correlation between the Froude number and the dimensionless eigenvalues for experiment AE16.

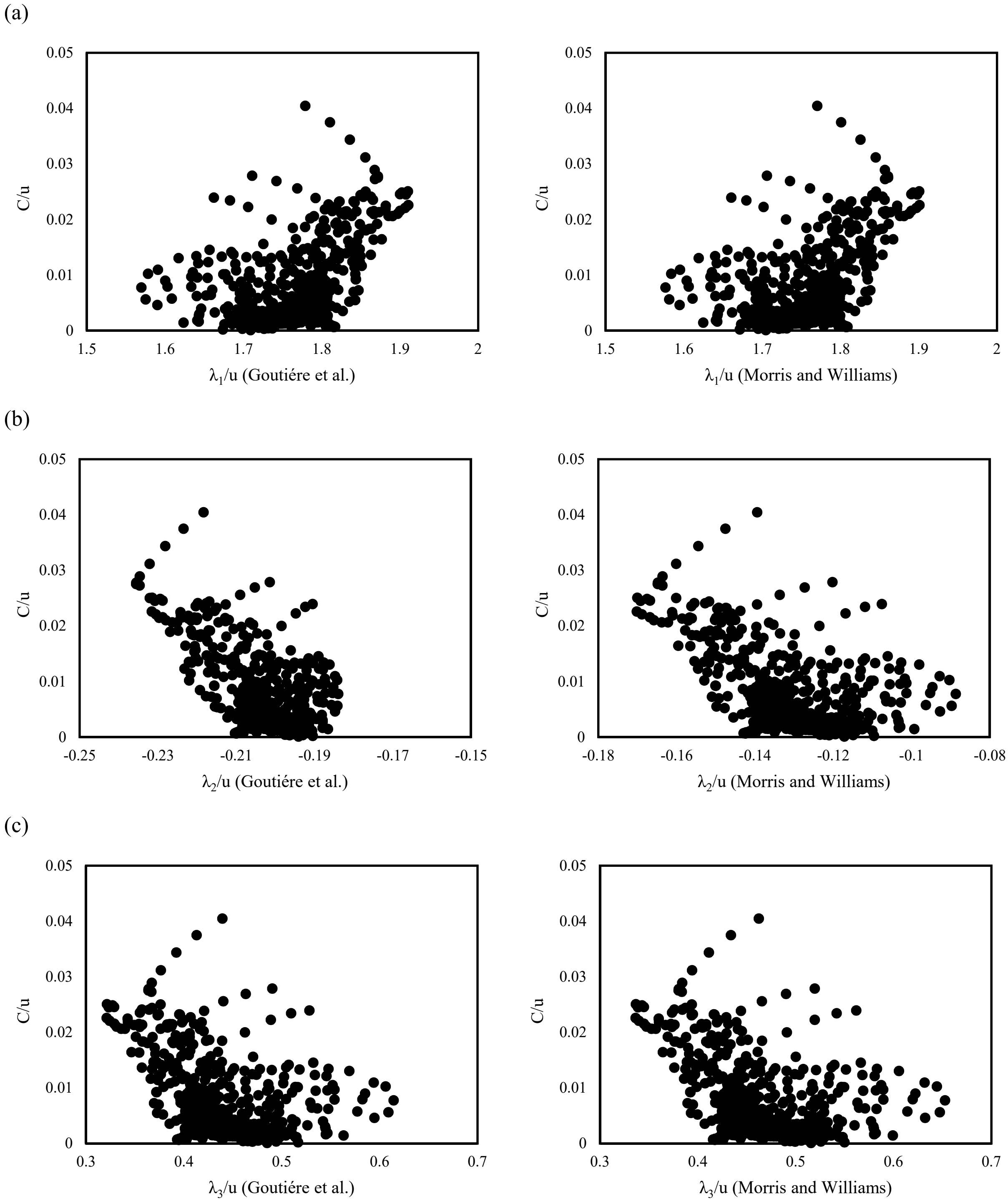

Figure S6. Scatter plots showing the correlations between the dimensionless eigenvalues and the dimensionless celerity of the aggradation wave for experiment AE16. The left graphs are obtained from the approximated solutions proposed by Goutière et al. (2008) and, the right graphs are derived from the exact solution of Morris and Williams' (1996) approach.

Table S4. Pearson's correlation coefficient between the dimensionless local and instantaneous celerity of the aggradation wave and the Froude number, as well as the dimensionless eigenvalues, for experiment AE17.

AE17		Goutière et al. (2008)			Morris and Williams (1996)		
	Fr	λ_1/u	λ_2/u	λ_3/u	λ_1/u	λ_2/u	λ_3/u
C/u	-0.47	0.50	-0.57	-0.47	0.50	-0.54	-0.47

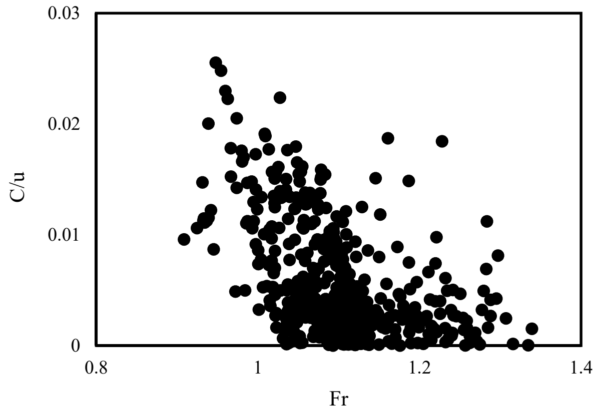

Figure S7. Scatter plot showing the correlation between the Froude number and the dimensionless local and instantaneous celerity of aggradation wave for experiment AE17.

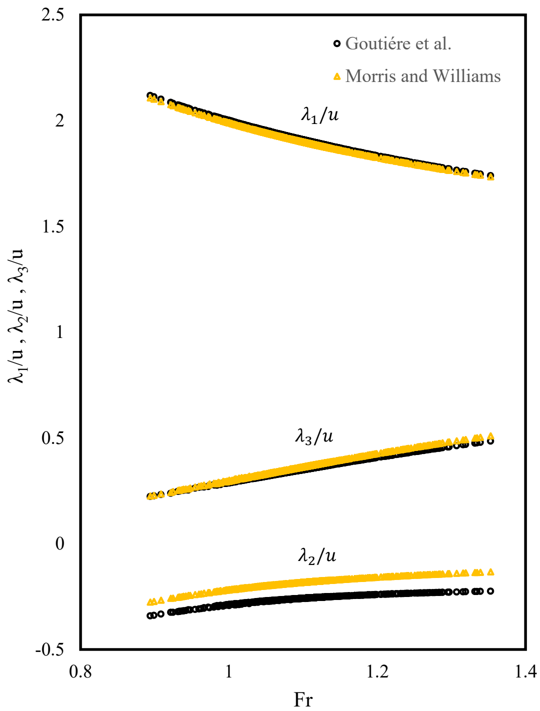

Figure S8. Scatter plot showing the correlation between the Froude number and the dimensionless eigenvalues for experiment AE17.

(a)

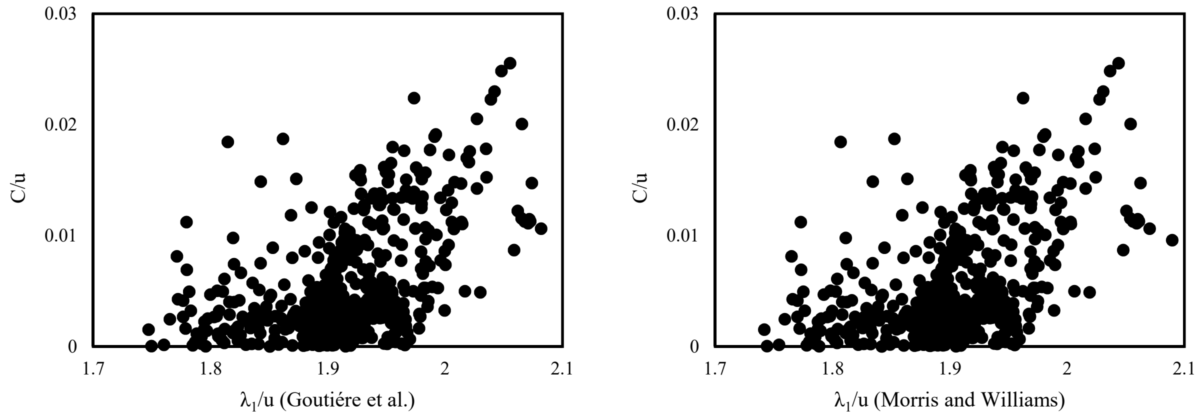

(b)

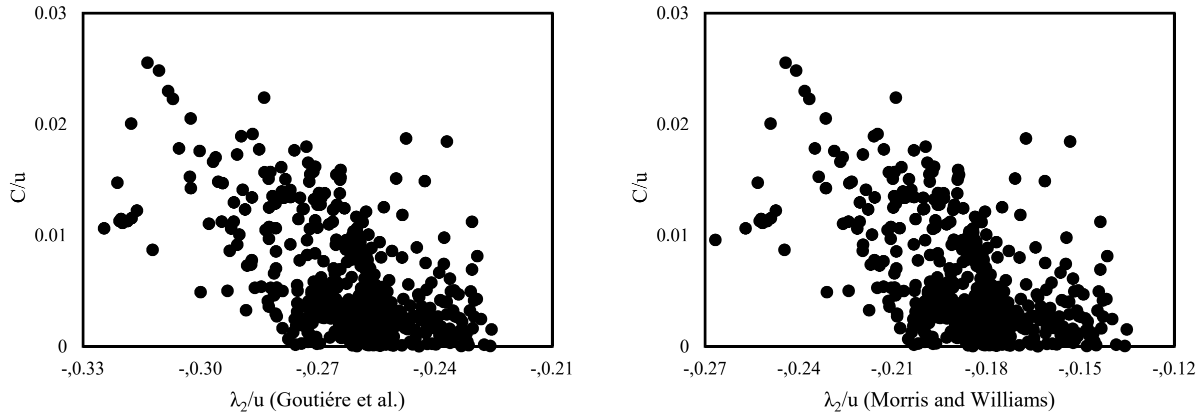

(c)

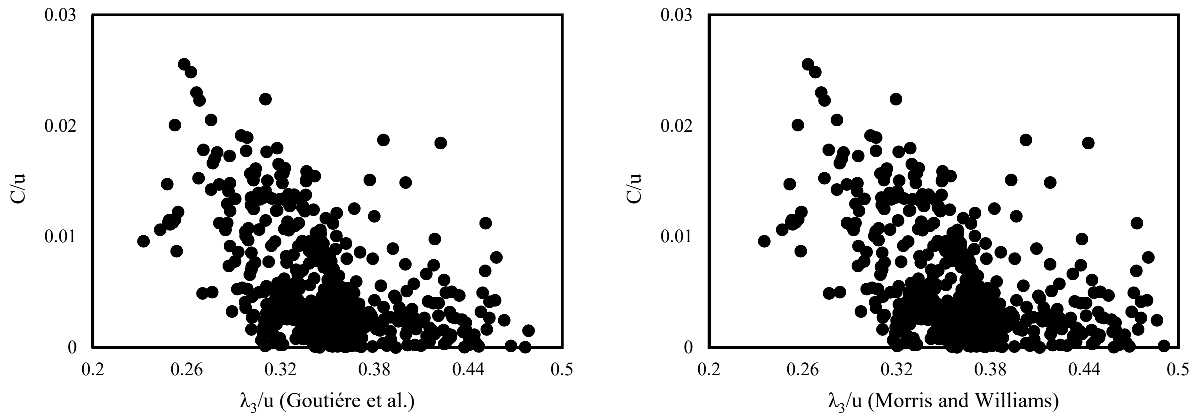

Figure S9. Scatter plots showing correlations between the dimensionless eigenvalues and the dimensionless celerity of the aggradation wave for experiment AE17. The left graphs are obtained from the approximated solutions proposed by Goutière et al. (2008) and, the right graphs are derived from the exact solution of Morris and Williams' (1996) approach.

Table S5. Pearson's correlation coefficient between the dimensionless local and instantaneous celerity of the aggradation wave and the Froude number, as well as the dimensionless eigenvalues, for experiment AE19.

AE19		Goutière et al. (2008)			Morris and Williams (1996)		
	Fr	λ_1/u	λ_2/u	λ_3/u	λ_1/u	λ_2/u	λ_3/u
C/u	-0.45	0.49	-0.58	-0.46	0.49	-0.53	-0.47

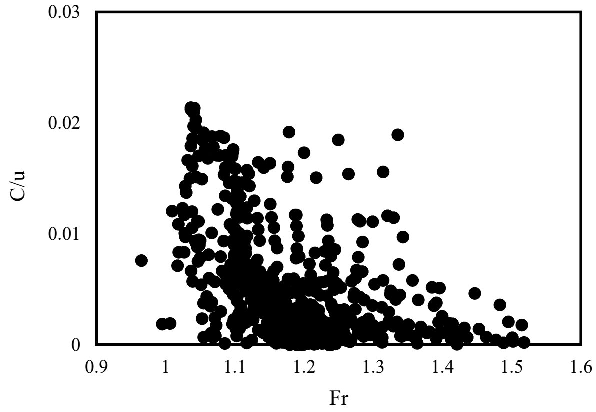

Figure S10. Scatter plot showing the correlation between the Froude number and the dimensionless local and instantaneous celerity of aggradation wave for experiment AE19.

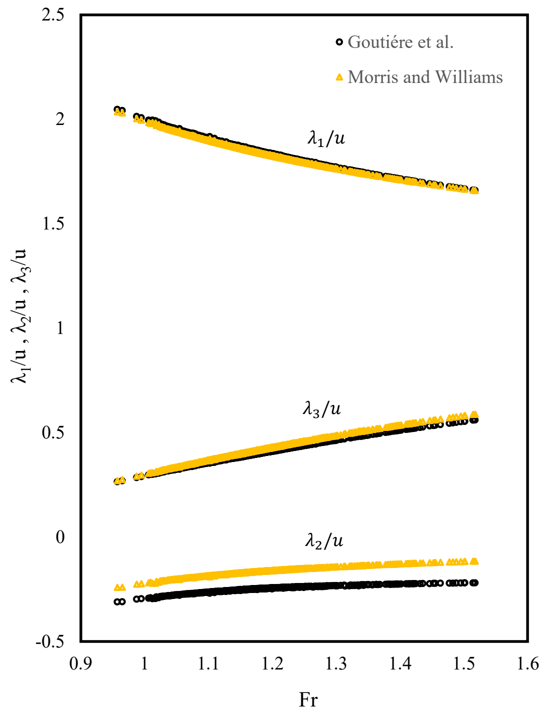

Figure S11. Scatter plot showing the correlation between the Froude number and the dimensionless eigenvalues for experiment AE19.

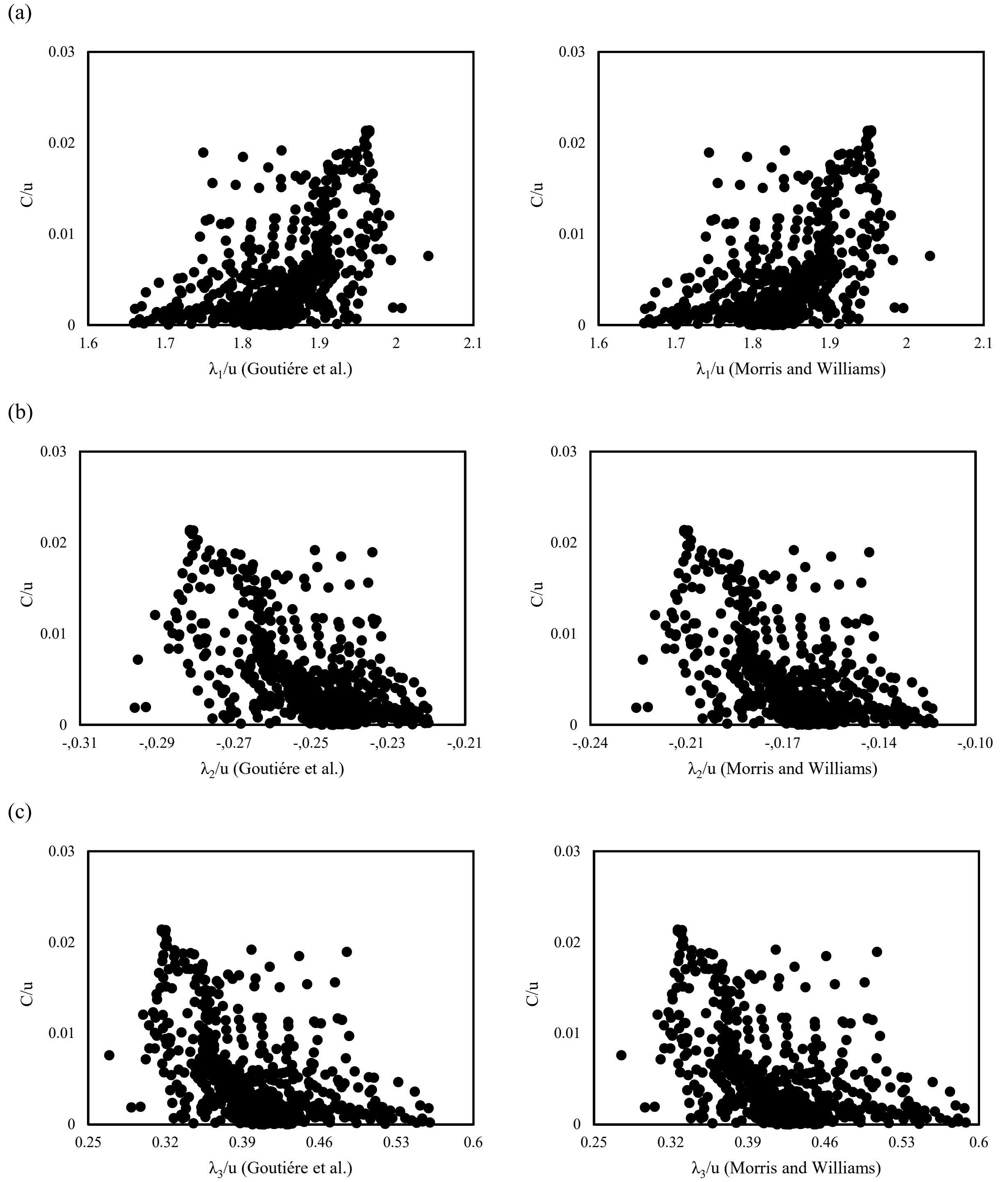

Figure S12. Scatter plots showing the correlations between the dimensionless eigenvalues and the dimensionless celerity of the aggradation wave for experiment AE19. The left graphs are obtained from the approximated solutions proposed by Goutière et al. (2008) and, the right graphs are derived from the exact solution of Morris and Williams' (1996) approach.

Table S6. Pearson's correlation coefficient between the dimensionless local and instantaneous celerity of the aggradation wave and the Froude number, as well as the dimensionless eigenvalues, for experiment AE24.

AE24		Goutière et al. (2008)			Morris and Williams (1996)		
	Fr	λ_1/u	λ_2/u	λ_3/u	λ_1/u	λ_2/u	λ_3/u
C/u	-0.34	0.37	-0.39	-0.36	0.37	-0.39	-0.36

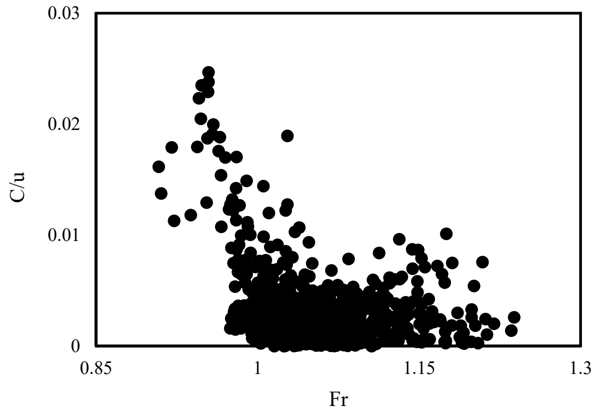

Figure S13. Scatter plot showing the correlation between the Froude number and the dimensionless local and instantaneous celerity of aggradation wave for experiment AE24.

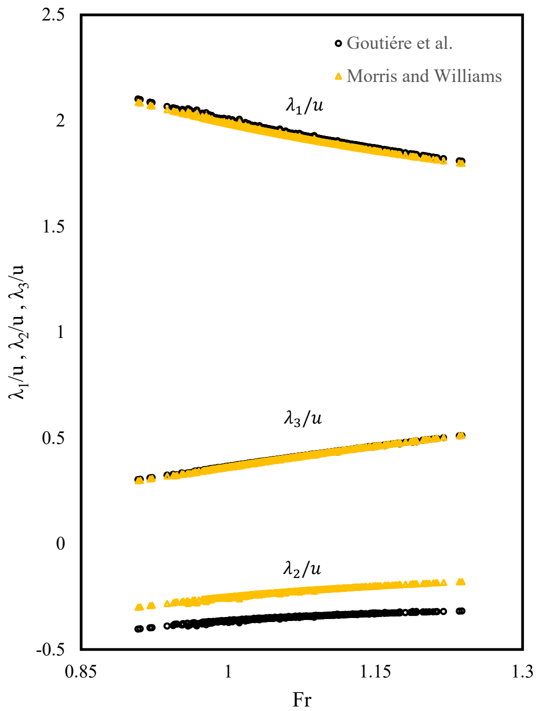

Figure S14. Scatter plot showing the correlation between the Froude number and the dimensionless eigenvalues for experiment AE24.

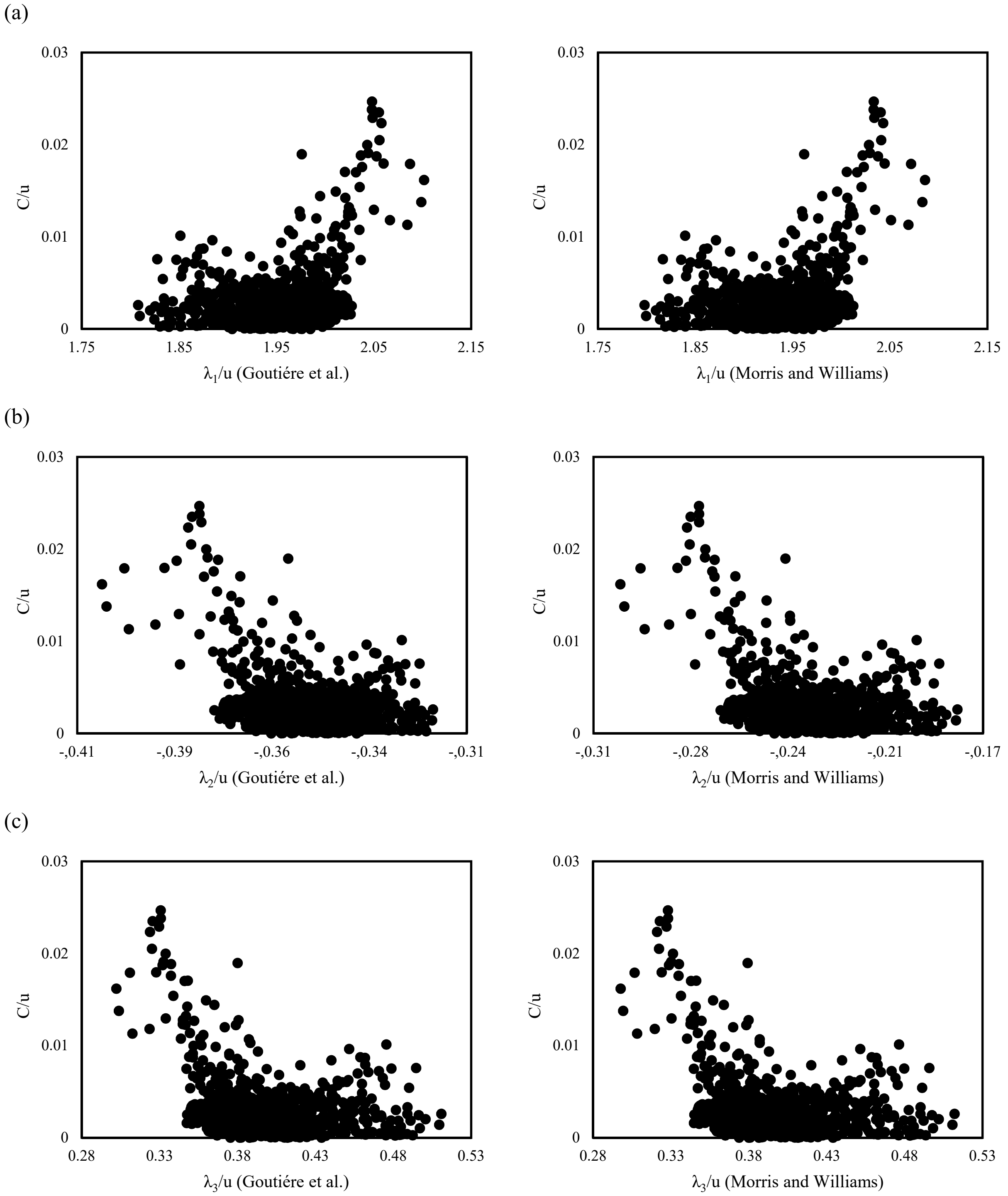

Figure S15. Scatter plots showing the correlations between the dimensionless eigenvalues and the dimensionless celerity of the aggradation wave for experiment AE24. The left graphs are obtained from the approximated solutions proposed by Goutière et al. (2008) and, the right graphs are derived from the exact solution of Morris and Williams' (1996) approach.

Examining the results of the five experiments, it can be observed that the trends between Fr and C/u, Fr and λ_i/u, and λ_i/u and C/u remain consistent across the experiments. As discussed in the paper for AE16: (i) a general decrease in dimensionless celerity is observed with increasing Froude number; (ii) C/u increases with λ_1/u and $|\lambda_2|/u$ and decreases with λ_3/u; and (iii) the values obtained for λ_2 differ depending on whether sediment concentration is considered or disregarded. Moreover, the values of the Pearson's correlation coefficient for all plots range between around 0.3 and 0.6, indicating a moderate correlation between the variables.

Finally, to show the consistency in the trends between the variables across the experiments, Fig. S16 presents scatter plots showing the correlation between Fr and C/u for all the performed runs (corresponding P values in Table S1). As observed, most of the experiments exhibit a similar trend, with C/u decreasing as Fr increases.

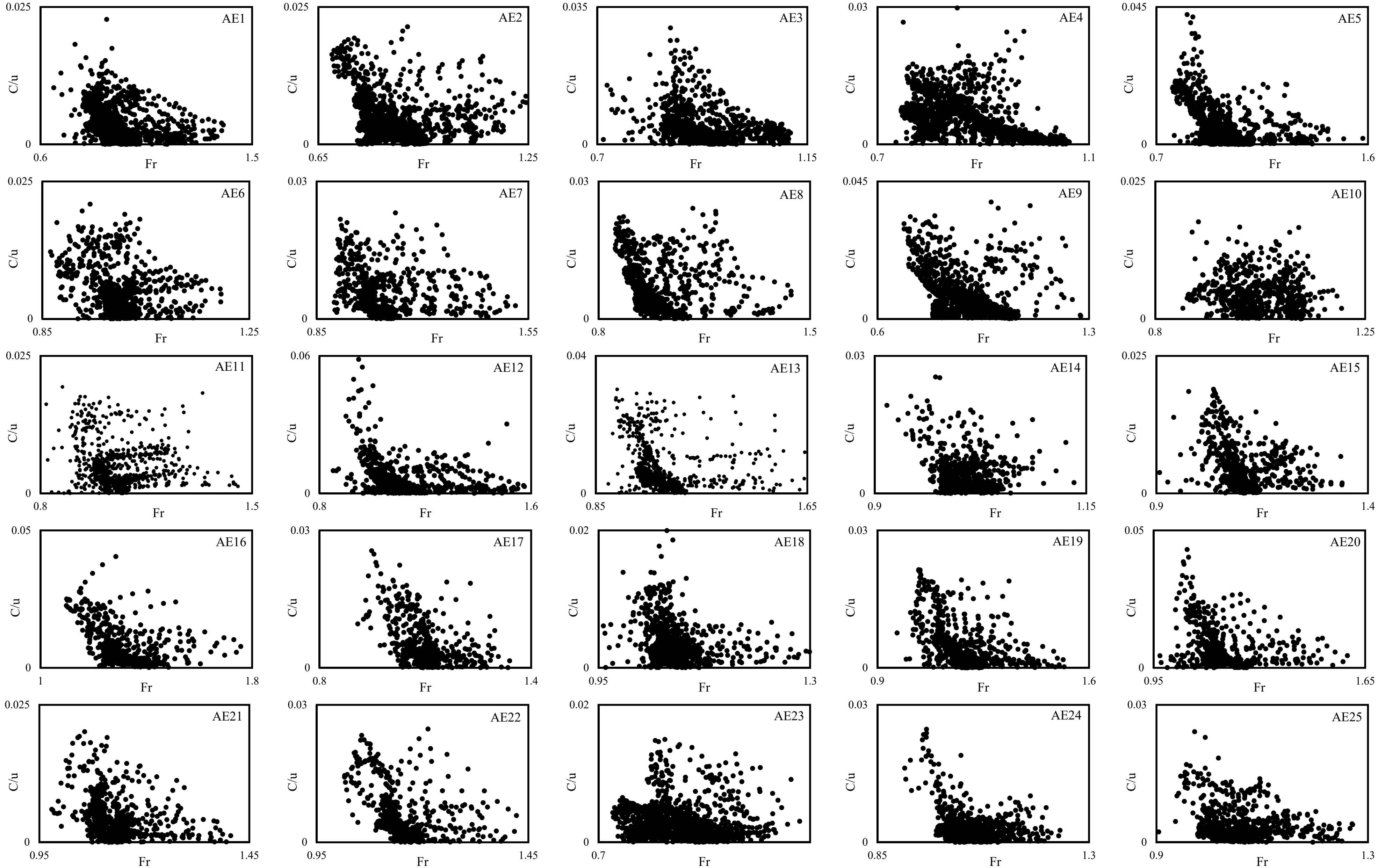

Figure S16. Scatter plots showing the correlation between the Froude number and the dimensionless local and instantaneous celerity of aggradation wave for all the performed experiments.